Czech Technical University in Prague
Faculty of Electrical Engineering - Dept. of Electromagnetic Field
www.elmag.org

Wireless Friendly Energy Efficient Buildings (WiFEEB)

Internal Draft Report on WP1 measurements at CTU

Written by: Ondrej Moravek, Milan Prihoda, Pavel Pechac

Contents

1 Introduction

The measurement system for the free space transmission and reflection measurements at 10-70 GHz has been established using various configurations using vector network analyzer (VNA). We chose two different sets of antennas according to the frequency bands of interest: 5-50 GHz and 50-75 GHz. The mechanical setup was optimized to accommodate 600×600 mm large samples. The geometrical setup can be further adjusted using absorbers. More information about measurement setup will be given in the following section.

1.1 List of materials

Code	Description	Nominal thickness (mm)	Estimated relative permittivity [1]
001	sound shield	15	$2.7 - j0.03$
002	sound shield	15	$2.7 - j0.03$
101	sound shield	12.5	$2.7 - j0.03$
102	sound shield	12.5	$2.7 - j0.03$
201	base board	9.5	$2.1 - j0.02$
202	base board	9.5	$2.1 - j0.02$
301	wall board	12.5	$2.2 - j0.01$
302	wall board	12.5	$2.2 - j0.01$
401	fire shield	12.5	$2.6 - j0.02$
402	fire shield	12.5	$2.6 - j0.02$
501	insulation shield	50	$1.03 - j0.002$
707	insulation shield	25	$1.03 - j0.002$
601	fire shield	9.5	$2.2 - j0.02$
602	fire shield	9.5	$2.2 - j0.02$
B1	MDF board	6	$2.4 - j0.15$
B2	MDF board	6	$2.4 - j0.15$
B3	plywood board	9	$2.4 - j0.15$
B4	plywood board	9	$2.4 - j0.15$
B5	chipboard	12	$1.85 - j0.15$
B6	chipboard	12	$1.85 - j0.15$
G1	glass	4	6.5 [2]
G2	glass	8	6.5 [2]
-	concrete slab	52	–

2 Measurement setup

The measurement setup is based on Rohde&Schwarz ZVA67 [3] VNA with time-domain option and two horn antennas for each frequency band. The setup was optimized throughout the year to achieve the best possible repeatability and confidence in our results. The free-space measurement approach was used mainly because the sample dimensions constraints, but its worth to note that there are several other possibilities of permittivity measurement [4].

The first band 10 - 50 GHz was measured using two double-ridged waveguide horn antennas from RFspin [5]. These antennas are fitted with 2.4mm coaxial connectors for which we used suitable cables and adapters. These components are shown in Fig. 1.

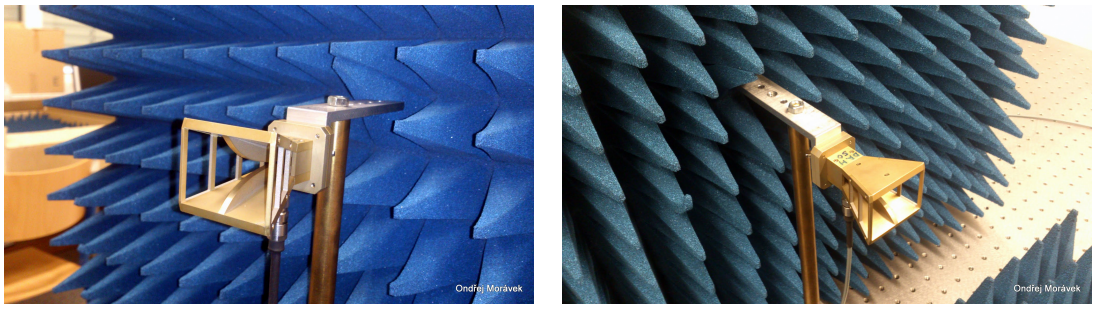

(a) RFspin DRH50 (b) RFspin DRH50

Figure 1: DRH50 - Double-ridged waveguide horn antennas by RFspin [5].

The WR-15 simple horn antennas were made in-house and their aperture D is approximately 26 mm. Additionally, we used two transitions [6] from WR-15 to V-connector (1.85mm) made by Radiometer Physics GmbH. These components are shown in more detail in the Fig. 2.

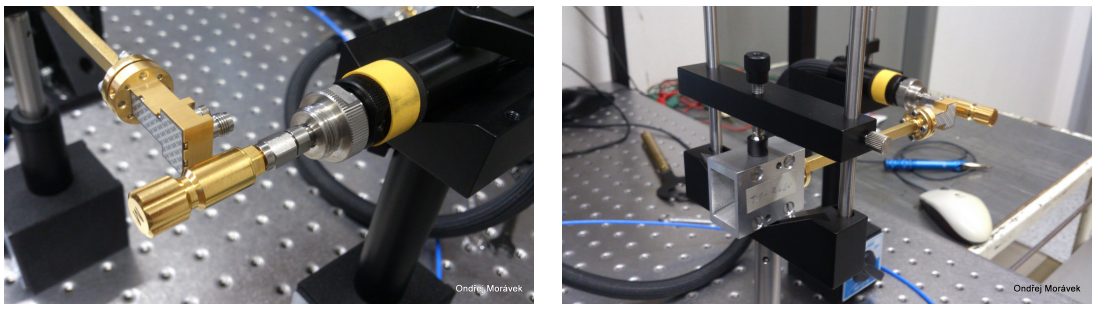

(a) WCA-75 waveguide to coaxial transition (b) WR-15 horn antenna

Figure 2: WR-15 horn antennas and transitions [6] from WR-15 to V-connector (1.85mm) made by Radiometer Physics GmbH.

The sample holder with all other equipment is mounted on to a optical table to maintain fixed position and repeatable translations of all components. We tried to vary several options of the setup configuration to evaluate their influence on the measured data to see if we can find an optimum. We have a list of the contributing factors which we think would influence the results:

- distance of the antennas from the sample

- multipath propagation and usage of absorbers
- properties of the reference metal sheet
- type of sample holder (i.e. maintaining sample flatness)
- types of measurement cables and connectors

The influence of each contributing factor will be discussed in the final section of this report. We were finally able to measure all samples in both frequency bands (some of them with limitations). All setups which were used during the experiments are shown in Fig. 3.

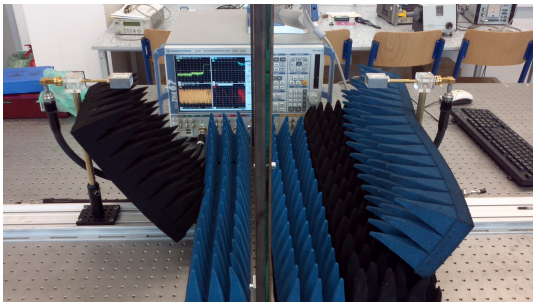

(a) Setup for V band with glass sample G1

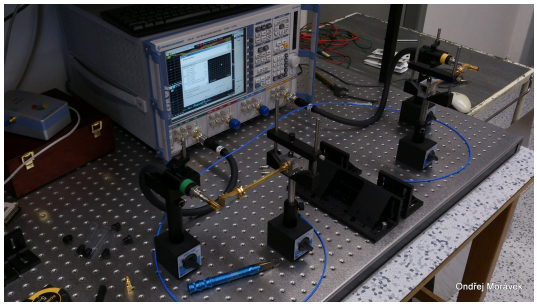

(b) Setup for V band

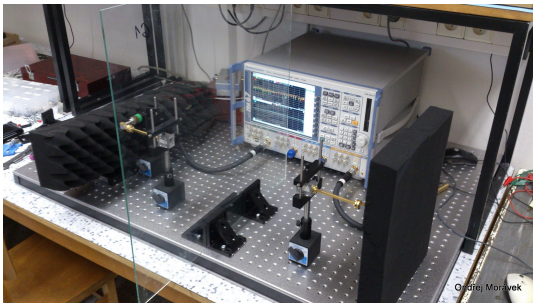

(c) Glass sample G1 in V band

(d) Setup for 50 GHz band

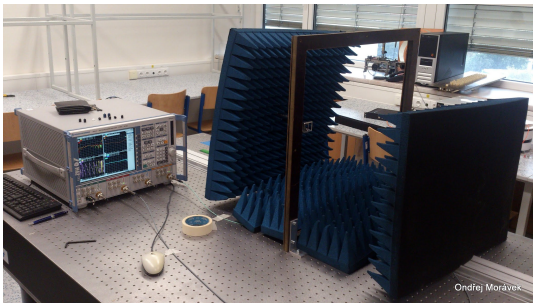

(e) Setup for 50 GHz band

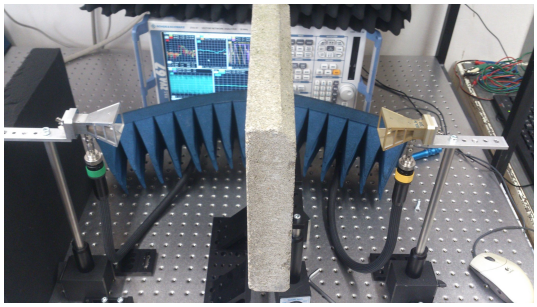

(f) Concrete sample in 50 GHz band

Figure 3: Various measurement setups.

3 Calibration and measurement methods

The software post-processing of the measured data which is necessary to obtain the desired values of complex permittivity has become one of the most important components of the measurement and data acquisition chain. After some experimental work and literature research we arrived to the following calibration scheme. The associated data processing chain can be divided into three parts:

1. Calibration and correction at the coaxial connector reference plane (using 2.4 or 1.85mm calibration kit)
2. Calibration of the measured data using gated-reflect-line (GRL) [7] method.
3. Extraction [9], [10] of the complex permittivity from the transmission and reflection data.

3.1 Calibration at the coaxial connectors

For the purpose of calibrating VNA at the antenna coaxial connectors we used very well known calibration methods short-open-load-thru (SOLT) and short-open-load-reciprocal (SOLR) [8]. Both methods are implemented in the VNA's firmware. This calibration was performed before the actual measurement of the samples. Then, we obtained corrected S-parameters for all measured samples.

During all measurements and for all setups, we tried to maintain consistent configuration of the VNA to achieve good reproducibility of our results. More specifically: IF bandwidth 100 Hz, number of points 1601/801, output power $0 \div 10$ dBm.

3.2 Gated-Reflect-Line calibration

The "gated-reflect-line" technique described in [7] was implemented in MATLAB to provide the post-processing mathematical background needed to calibrate and correct the measured data into secondary reference plane located at the edges of the metal sheet which is used as a reference reflection standard. For more details about the reference planes and the measurement configuration, see the schematic in Fig. 4.

This technique is a derivative of TRL [11] which was published in 1979. The GRL simplifies the approach by using only two calibration standards (free-space and metal sheet). The remaining unknowns are extracted from the free-space calibration measurement by means of time-gating and forward/inverse Fourier transformations of the reflections. If we gate-out the measured S_{11} at the coaxial calibration reference plane, we will see two reflected signals separated in time: first peak from the connector and aperture of the first antenna and second peak from the aperture of the second antenna. If the separation is long enough, we can time-gate the first reflected wave, convert is back into frequency domain and save the data as reflection coefficient (S'_{11}) of the input error model.

The Hamming window and gating functions along with carefully picked gating time span were chosen to perform the transformations and gating as they provided the most satisfying results.

The reference reflection from the metal sheet (which is assumed to have $\Gamma_{\text{metal}} = -1$) is then used to extract remaining unknowns in both error models. The properties of the metal

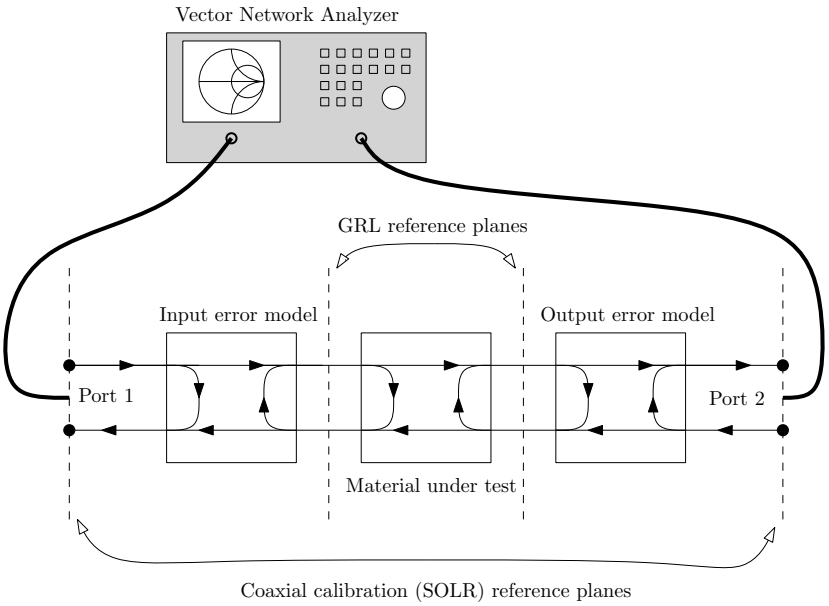

Figure 4: Schematic of the measurement and GRL calibration setup with highlighted reference planes.

are very important (flatness, conductivity, thickness) and this calibration measurement will set our GRL reference planes which will be at the edges of the metal.

The material under test (MUT) can be now placed into the sample holder. This method assumes that thickness of the metal sheet (t_{metal}) should be same as the thickness of the MUT. This is however impractical and it would require to have different metal sheet for each material. We can avoid this if we use one GRL reference plane constant (e.g. the left one) during all measurements. If we measure some MUT, which is thicker than the metal sheet, appropriate corrections will have to be made during the following extraction. The measured data of MUT with thickness t_1 will have incorrectly placed its calibration reference plane by an offset which is equivalent to length difference $t_1 - t_{\text{metal}}$. This could be resolved by proper de-embedding at the correct side of the reference plane.

3.3 Extraction of the complex permittivity

Extraction of the complex permittivity from the complex S-parameters is described generally in paper from NIST [10]. We implemented this approach in Matlab with some modifications which were published in [9].

This algorithm is based on solving a over-determined set of equations (i.e. optimization problem) where the measured data are used to provide solution data to a physical model which describes the problem as plane electromagnetic wave propagating though 3 layers of material with different properties (i.e. different ε_r). The material of interest is covered with two layers of air/vacuum with $\varepsilon_r = 1$. On each frequency point f, we are trying to find two unknowns - $\varepsilon_r'(f)$, $\varepsilon_r''(f)$.

There are different approaches available. Just to name one, we can solve the over-determined set of equations in the whole frequency range in one step. This introduces larger set of parameters and solutions. We could simplify the problem by providing a simple func-

tions with only few parameters, which would provide reliable physical representation of the real and imaginary parts of complex permittivity. This will provide faster and more robust fitting of the measured data, but we would have to have good confidence in the functions and their relationship to the real physical behaviour of the material.

Extraction of the complex permittivity for one material on 79 frequency points takes roughly one minute on a standard 64-bit desktop Windows PC. Example of the results for one specific material are shown in Fig. 5.

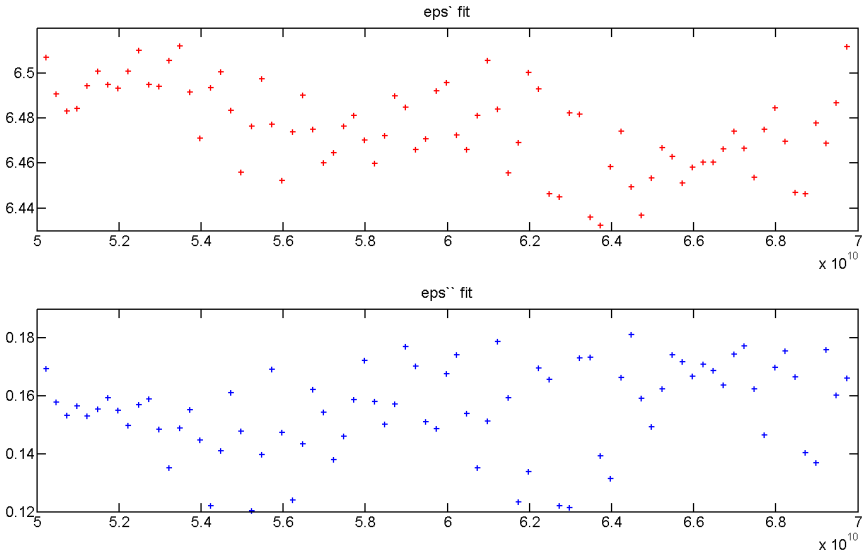

(a) Complex permittivity in the WR-15 band of the glass sample G2

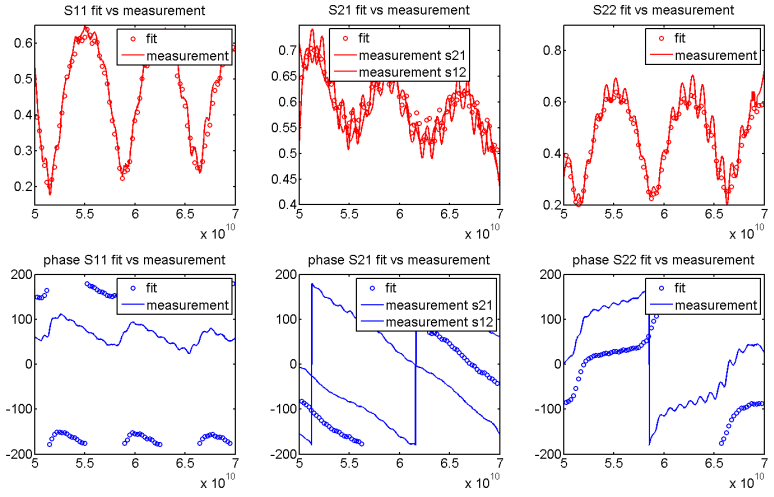

(b) Comparison between simulated (using fitted values) and raw measured S-parameters

Figure 5: Example of the extraction results for material G2.

Extracted complex permittivity results are used as parameters of the physical model to perform verification between the fit and measurement. The example in Fig. 5 shows magni-

tudes and angles of both reflection coefficients S_{11}, S_{22} and transmission S_{21}. The agreement between measurement and fit is sufficient, especially in the magnitude. The discrepancy between fitted and measured phase of the S-parameters is caused by several factors which will be discussed later. Main reason for this deviation is caused by inconsistencies between reference planes of the metal and measured MUT, which is difficult to maintain on higher frequencies.

4 Results

The presented results are in the form of frequency dependent complex permittivity which was extracted from measured data. Extracted real and imaginary parts of complex permittivity were fitted by a simple function af^b where f is frequency in Hz.

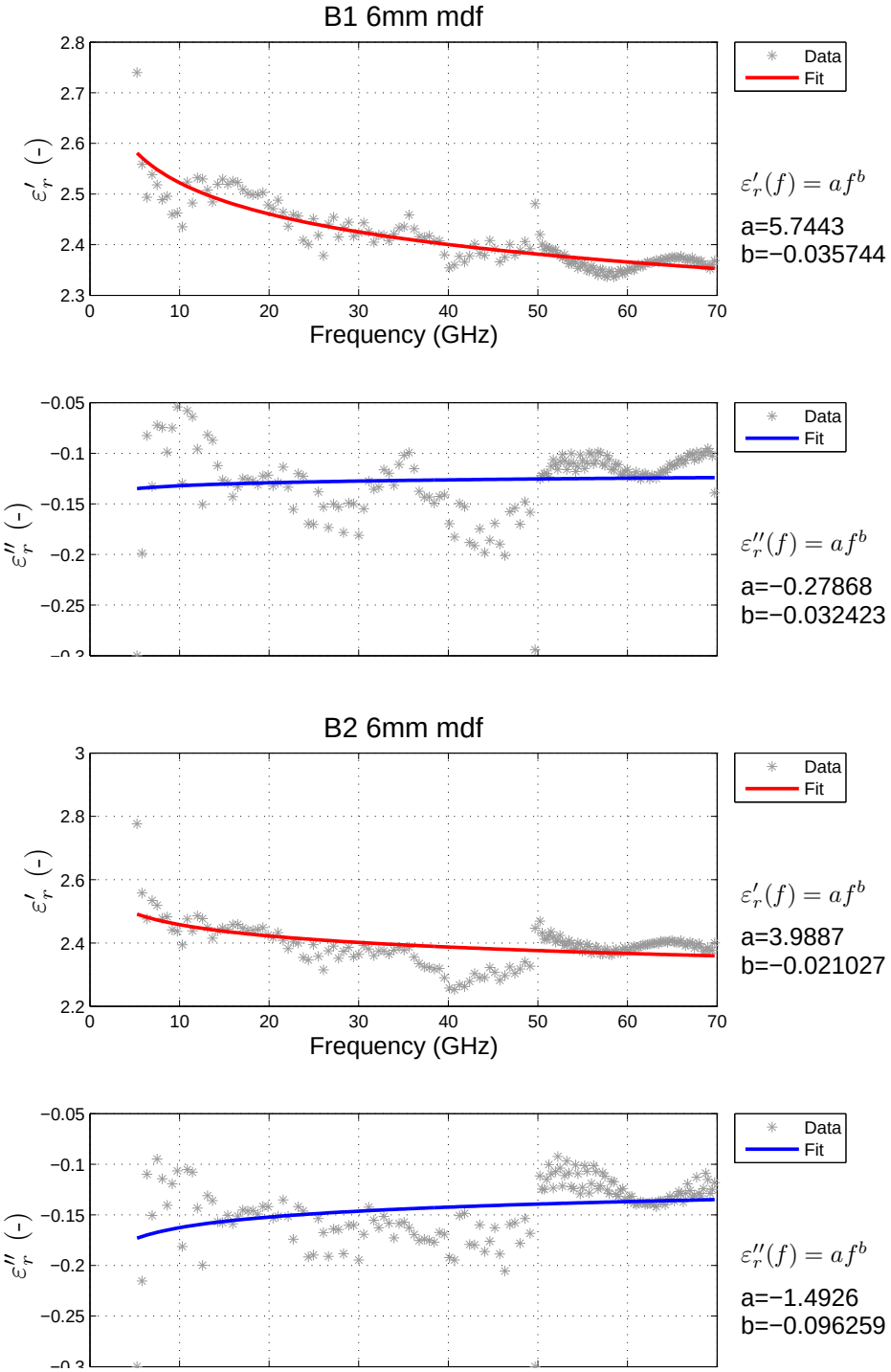

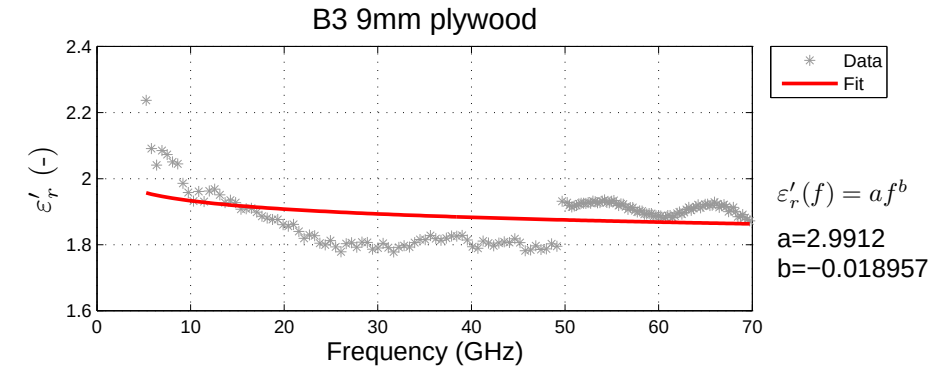
B3 9mm plywood
Data
Fit
ε_r' (-)
Frequency (GHz)
$\varepsilon_r'(f) = af^b$
a=2.9912
b=−0.018957

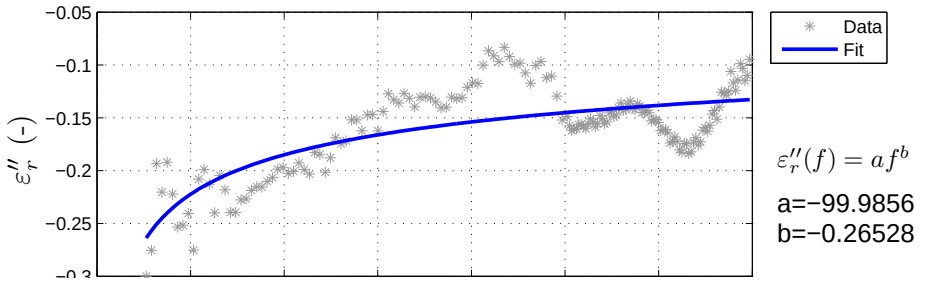
Data
Fit
ε_r'' (-)
$\varepsilon_r''(f) = af^b$
a=−99.9856
b=−0.26528

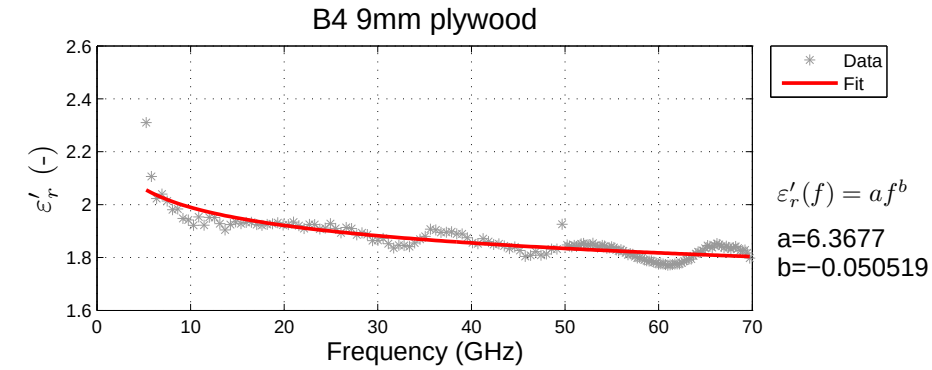
B4 9mm plywood
Data
Fit
ε_r' (-)
Frequency (GHz)
$\varepsilon_r'(f) = af^b$
a=6.3677
b=−0.050519

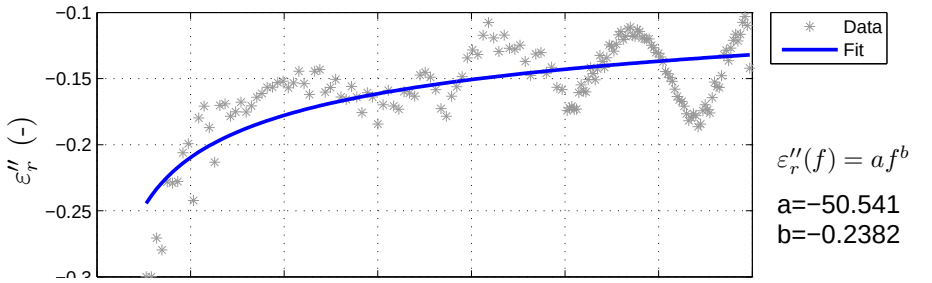
Data
Fit
ε_r'' (-)
$\varepsilon_r''(f) = af^b$
a=−50.541
b=−0.2382

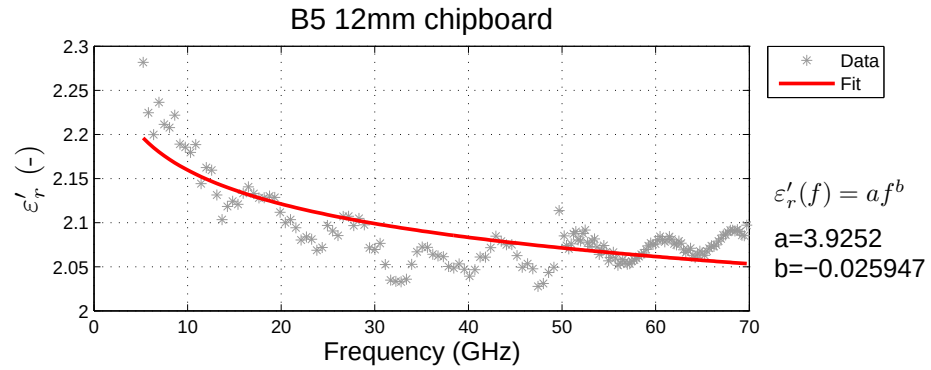
B5 12mm chipboard
Data
Fit
ε_r' (-)
Frequency (GHz)
$\varepsilon_r'(f) = af^b$
a=3.9252
b=−0.025947

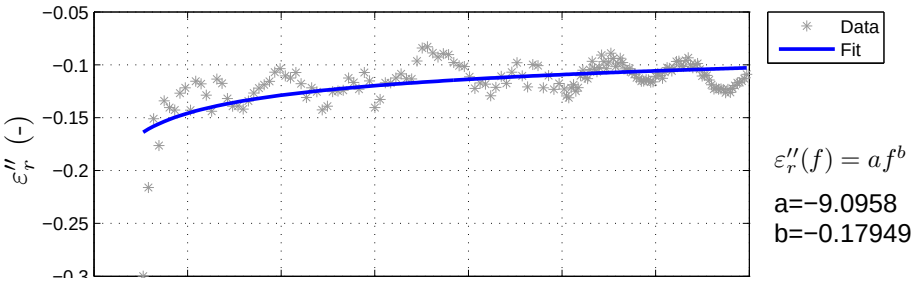
Data
Fit
ε_r'' (-)
$\varepsilon_r''(f) = af^b$
a=−9.0958
b=−0.17949

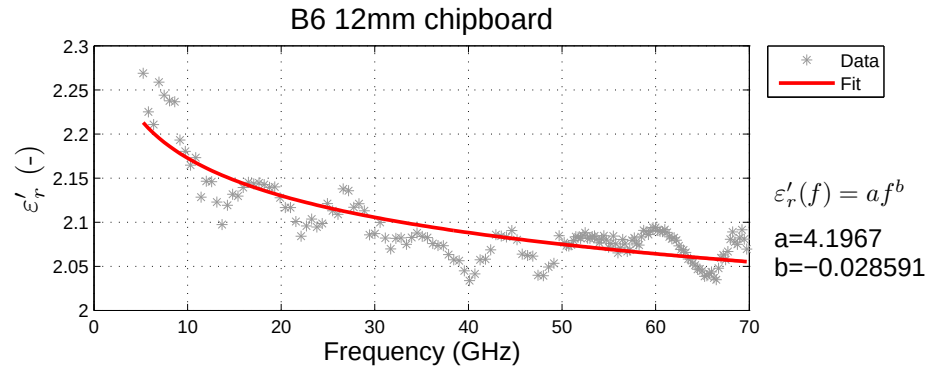
B6 12mm chipboard
Data
Fit
ε_r' (-)
Frequency (GHz)
$\varepsilon_r'(f) = af^b$
a=4.1967
b=−0.028591

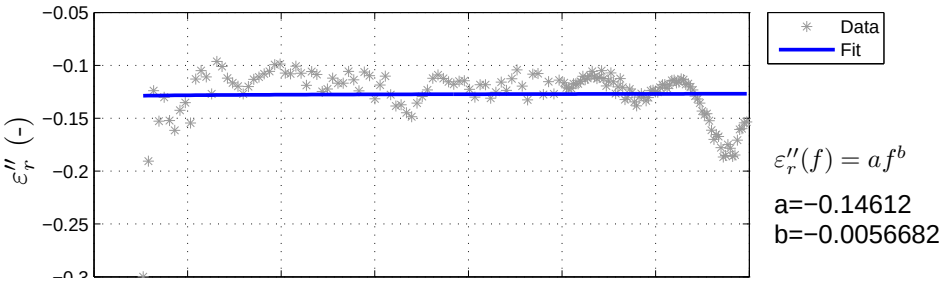
Data
Fit
ε_r'' (-)
$\varepsilon_r''(f) = af^b$
a=−0.14612
b=−0.0056682

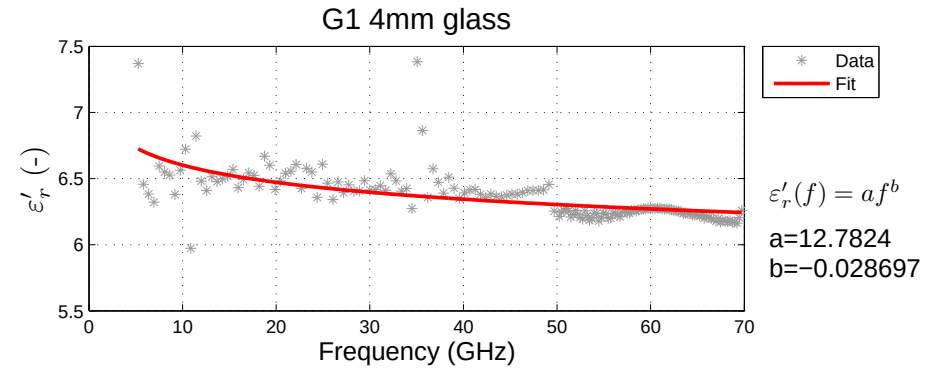
G1 4mm glass
Data
Fit
ε_r' (-)
Frequency (GHz)
$\varepsilon_r'(f) = af^b$
a=12.7824
b=−0.028697

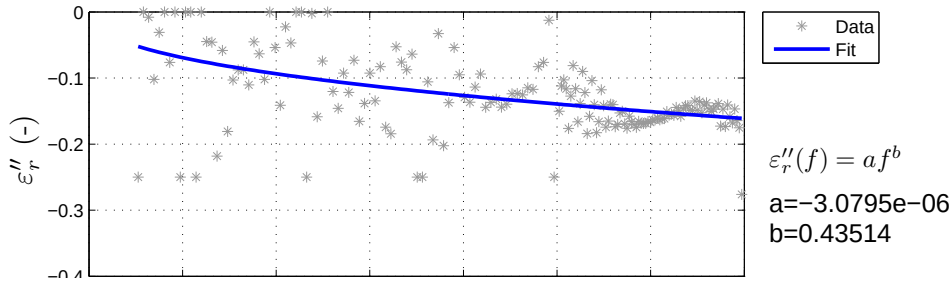
Data
Fit
ε_r'' (-)
$\varepsilon_r''(f) = af^b$
a=−3.0795e−06
b=0.43514

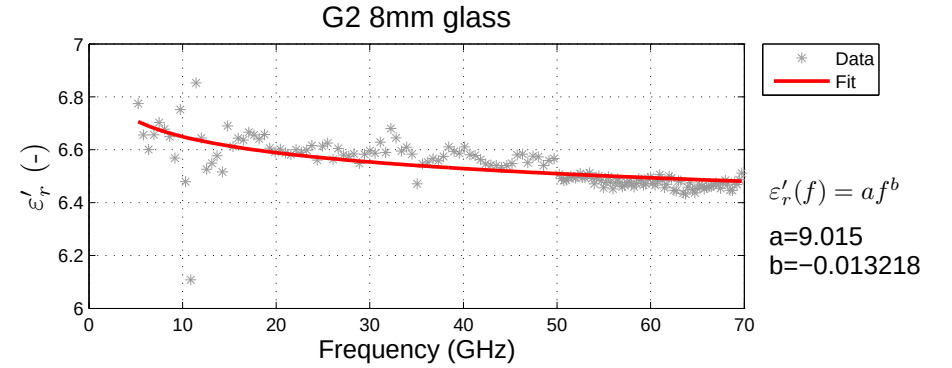
G2 8mm glass
Data
Fit
ε_r' (-)
Frequency (GHz)
$\varepsilon_r'(f) = af^b$
a=9.015
b=−0.013218

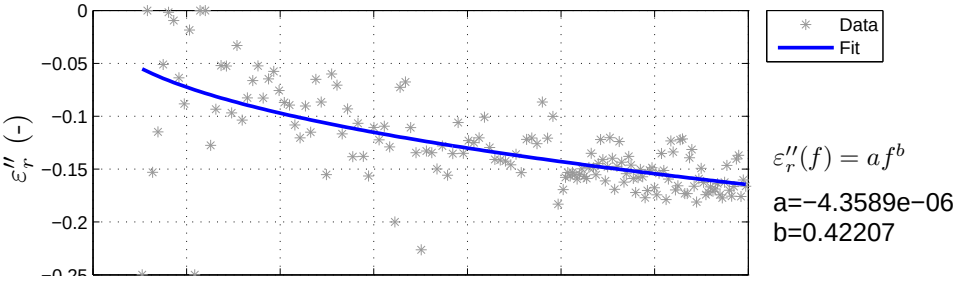
Data
Fit
ε_r'' (-)
$\varepsilon_r''(f) = af^b$
a=−4.3589e−06
b=0.42207

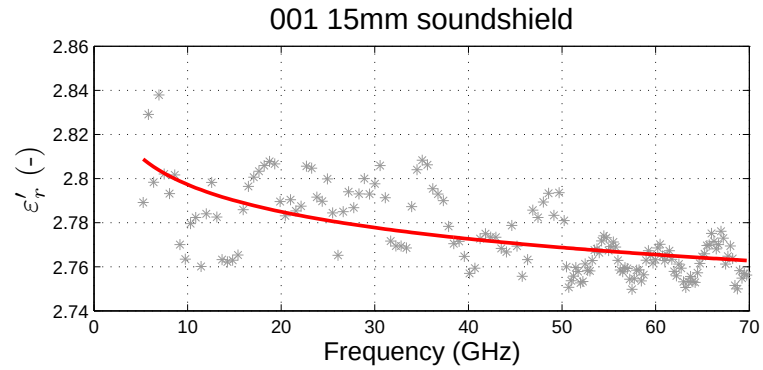

$\varepsilon_r'(f) = af^b$

a=3.2399

b=−0.0063798

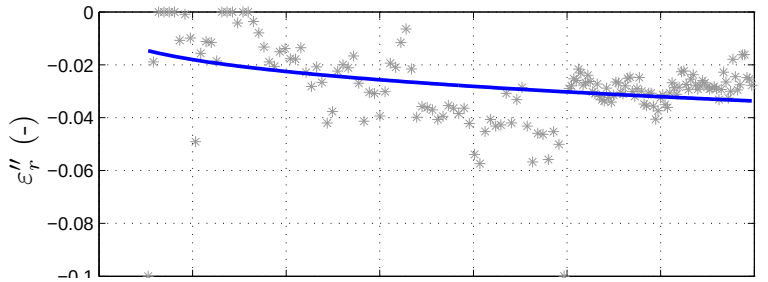

$\varepsilon_r''(f) = af^b$

a=−1.1041e−05

b=0.32131

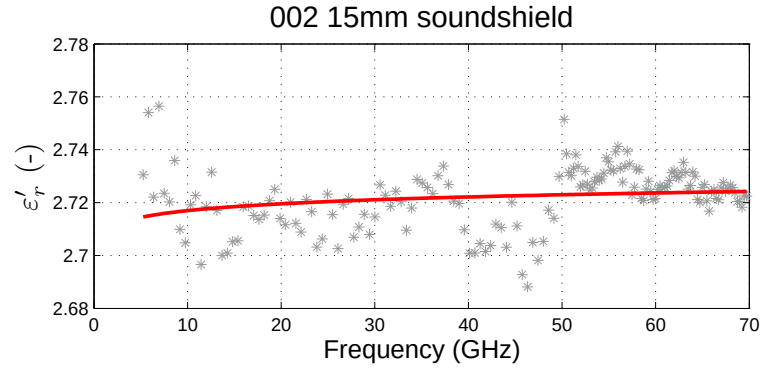

$\varepsilon_r'(f) = af^b$

a=2.6325

b=0.0013712

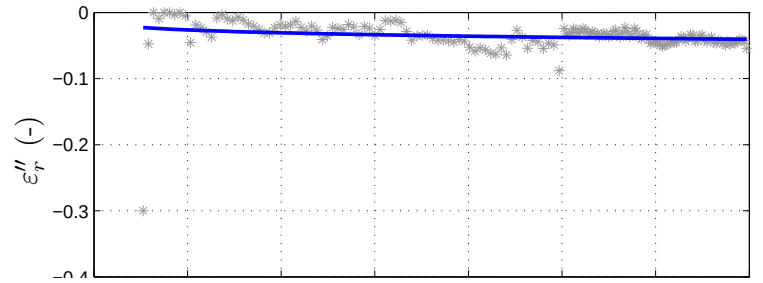

$\varepsilon_r''(f) = af^b$

a=−0.0001614

b=0.22128

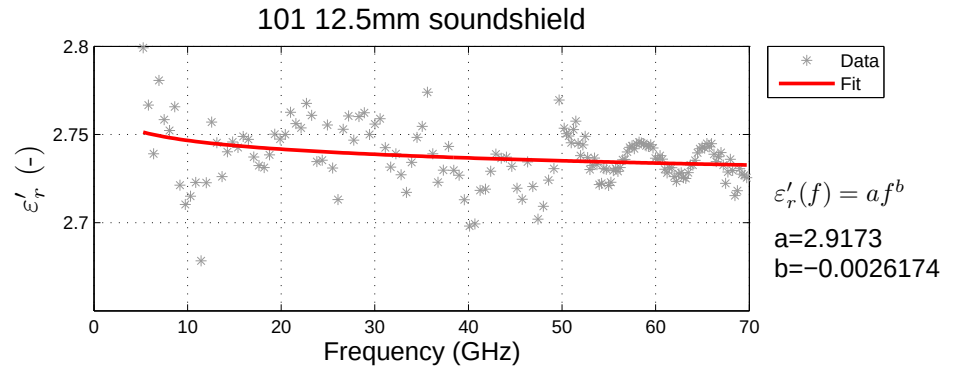
101 12.5mm soundshield
Data
Fit
ε_r' (-)
Frequency (GHz)
$\varepsilon_r'(f) = af^b$
a=2.9173
b=−0.0026174

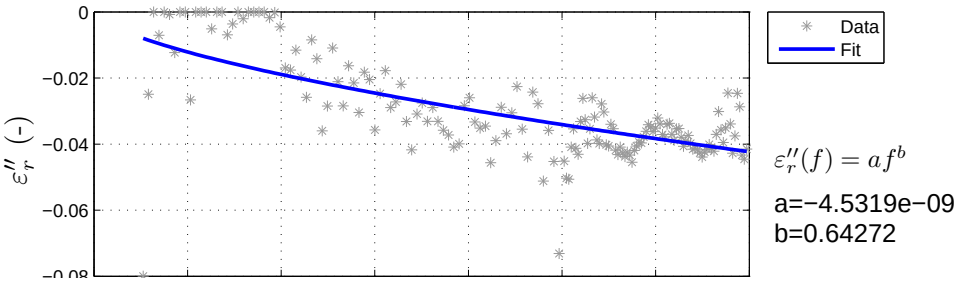
Data
Fit
ε_r'' (-)
$\varepsilon_r''(f) = af^b$
a=−4.5319e−09
b=0.64272

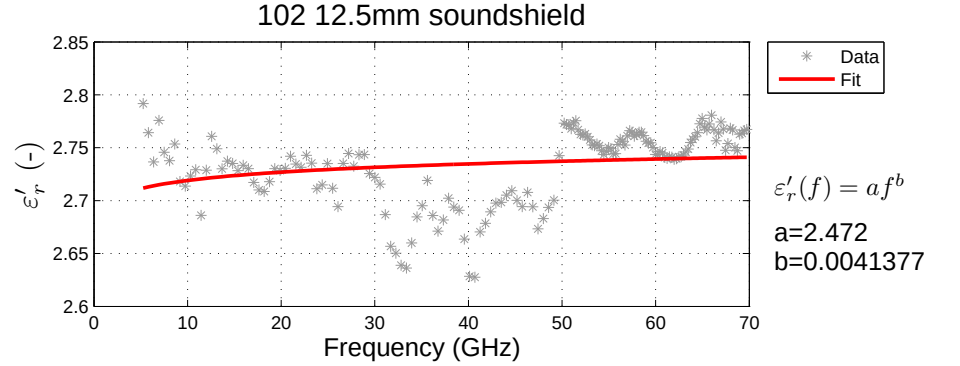
102 12.5mm soundshield
Data
Fit
ε_r' (-)
Frequency (GHz)
$\varepsilon_r'(f) = af^b$
a=2.472
b=0.0041377

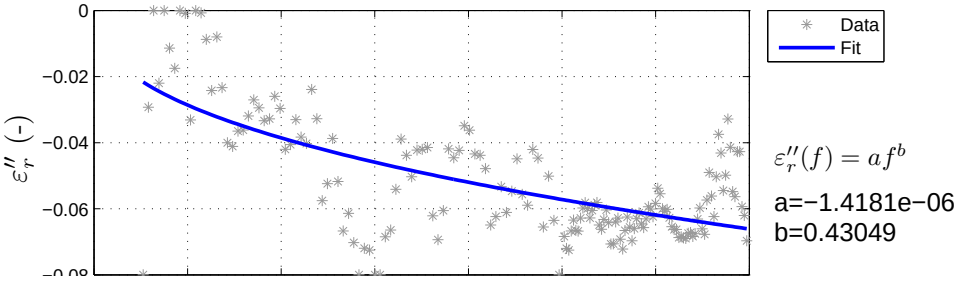
Data
Fit
ε_r'' (-)
$\varepsilon_r''(f) = af^b$
a=−1.4181e−06
b=0.43049

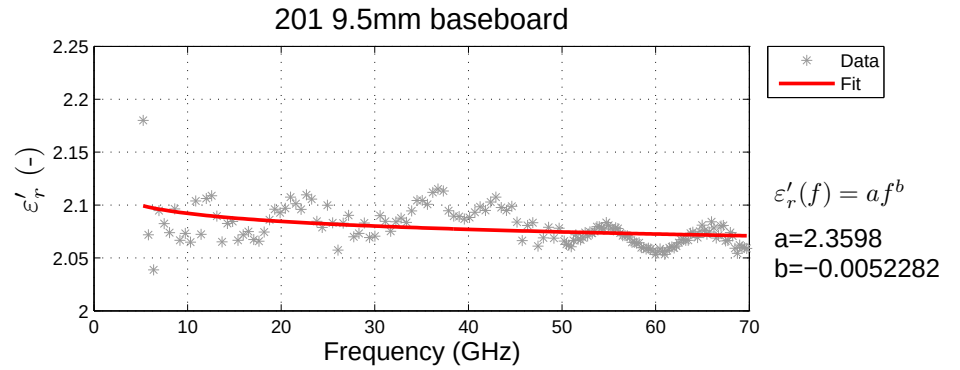
201 9.5mm baseboard
Data
Fit
ε_r' (-)
Frequency (GHz)
$\varepsilon_r'(f) = af^b$
a=2.3598
b=−0.0052282

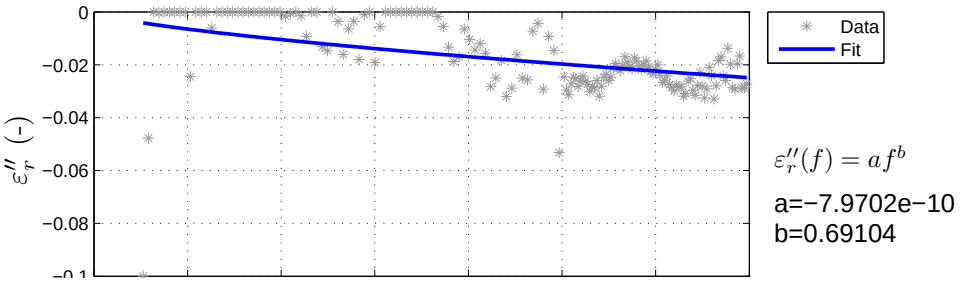
Data
Fit
ε_r'' (-)
$\varepsilon_r''(f) = af^b$
a=−7.9702e−10
b=0.69104

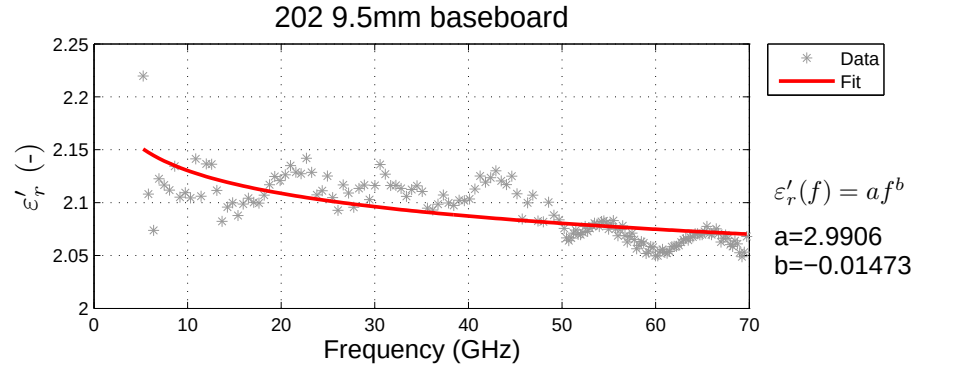
202 9.5mm baseboard
Data
Fit
ε_r' (-)
Frequency (GHz)
$\varepsilon_r'(f) = af^b$
a=2.9906
b=−0.01473

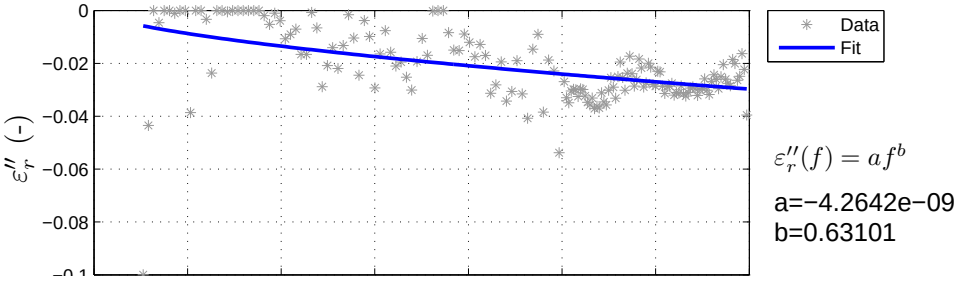
Data
Fit
ε_r'' (-)
$\varepsilon_r''(f) = af^b$
a=−4.2642e−09
b=0.63101

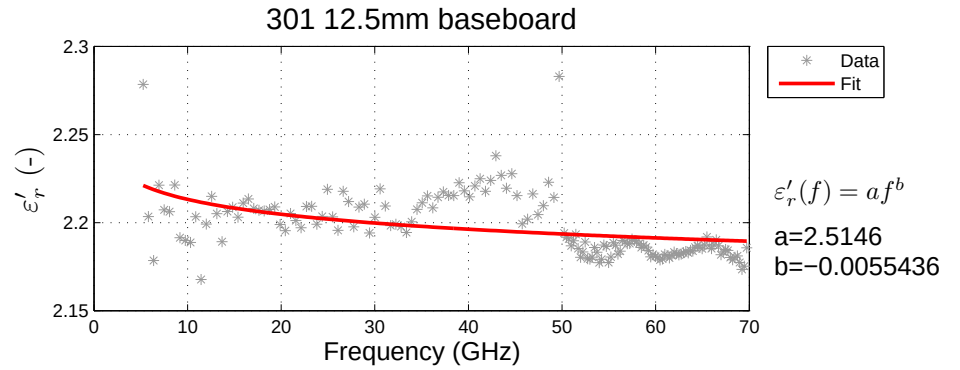
301 12.5mm baseboard
Data
Fit
ε_r' (-)
Frequency (GHz)
$\varepsilon_r'(f) = af^b$
a=2.5146
b=−0.0055436

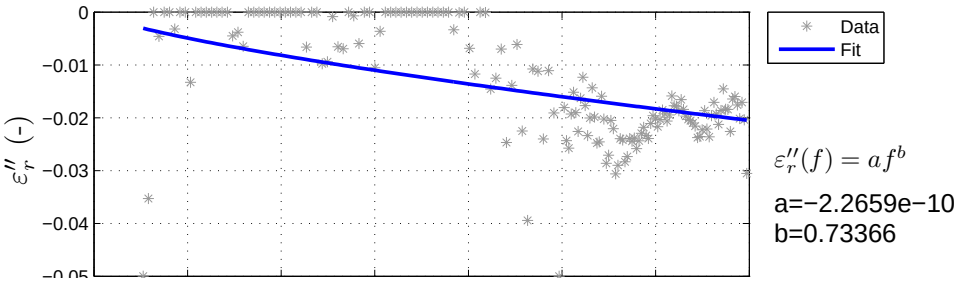
Data
Fit
ε_r'' (-)
$\varepsilon_r''(f) = af^b$
a=−2.2659e−10
b=0.73366

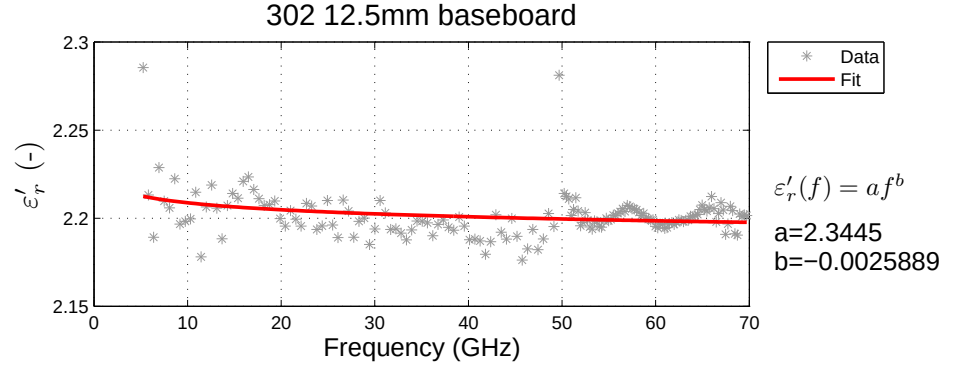
302 12.5mm baseboard
Data
Fit
ε_r' (-)
Frequency (GHz)
$\varepsilon_r'(f) = af^b$
a=2.3445
b=−0.0025889

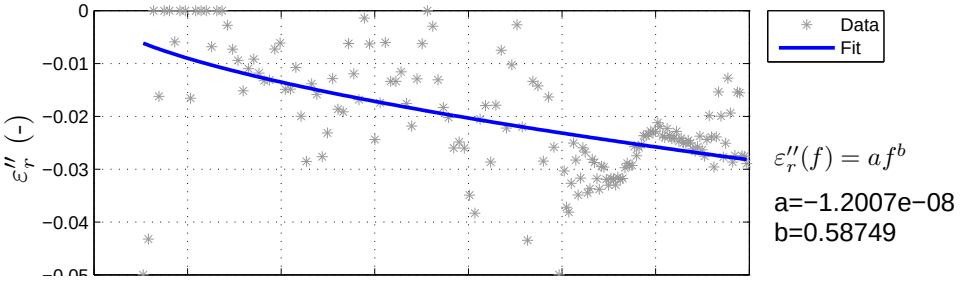
Data
Fit
ε_r'' (-)
$\varepsilon_r''(f) = af^b$
a=−1.2007e−08
b=0.58749

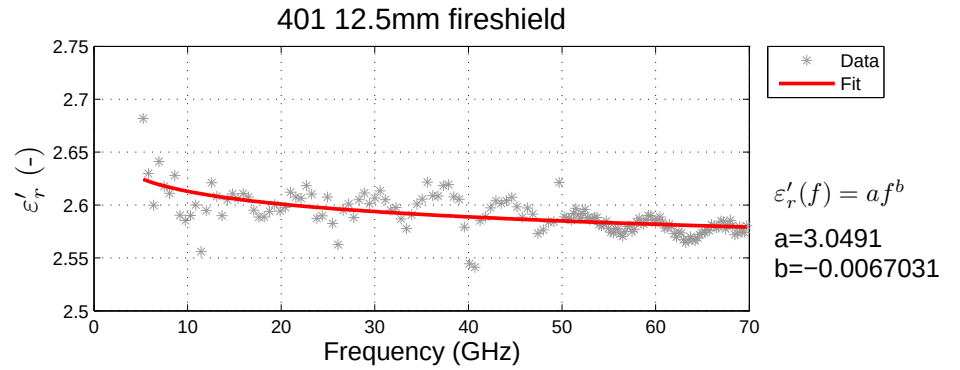
401 12.5mm fireshield
Data
Fit
ε_r' (-)
Frequency (GHz)
$\varepsilon_r'(f) = af^b$
a=3.0491
b=−0.0067031

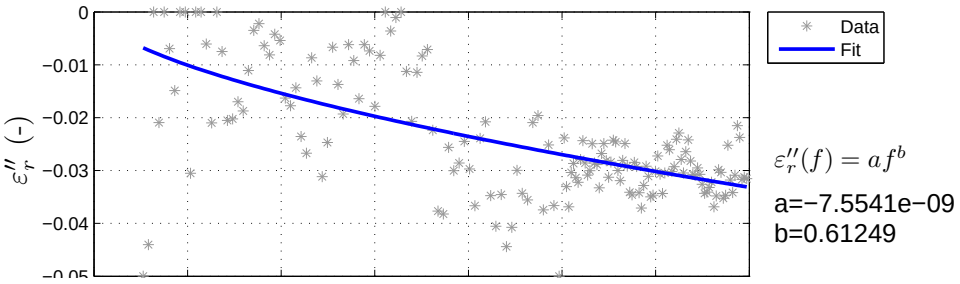
Data
Fit
ε_r'' (-)
$\varepsilon_r''(f) = af^b$
a=−7.5541e−09
b=0.61249

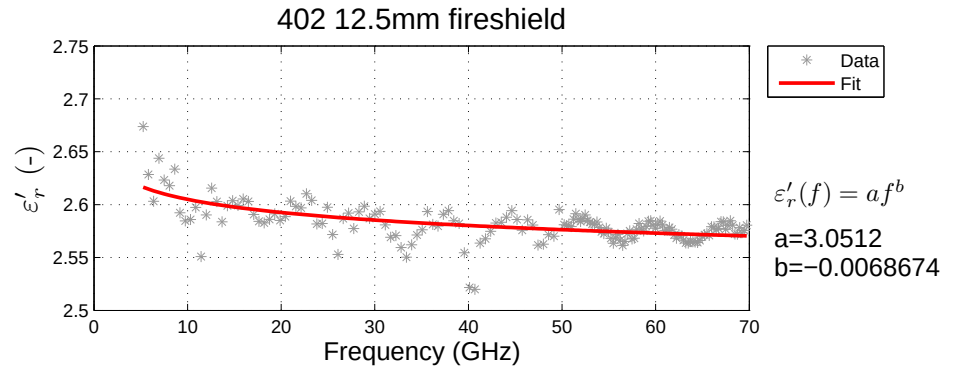
402 12.5mm fireshield
Data
Fit
ε_r' (-)
Frequency (GHz)
$\varepsilon_r'(f) = af^b$
a=3.0512
b=−0.0068674

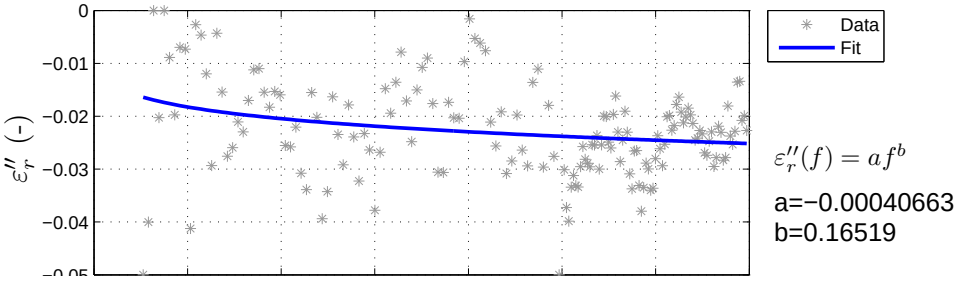
Data
Fit
ε_r'' (-)
$\varepsilon_r''(f) = af^b$
a=−0.00040663
b=0.16519

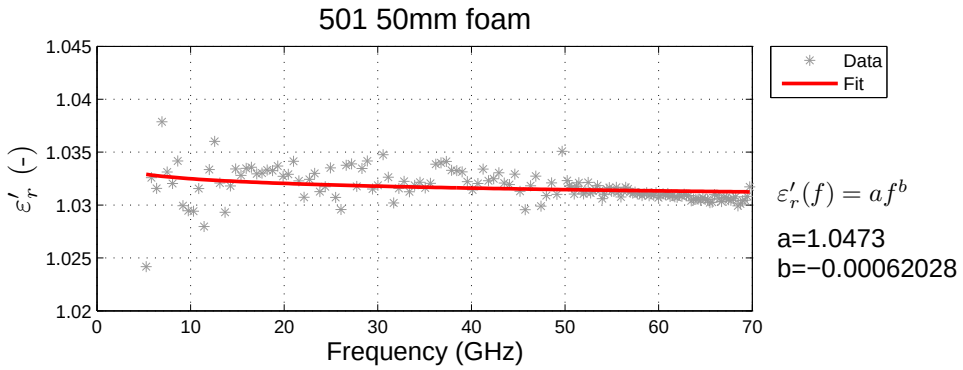
501 50mm foam
Data
Fit
ε_r' (-)
Frequency (GHz)
$\varepsilon_r'(f) = af^b$
a=1.0473
b=−0.00062028

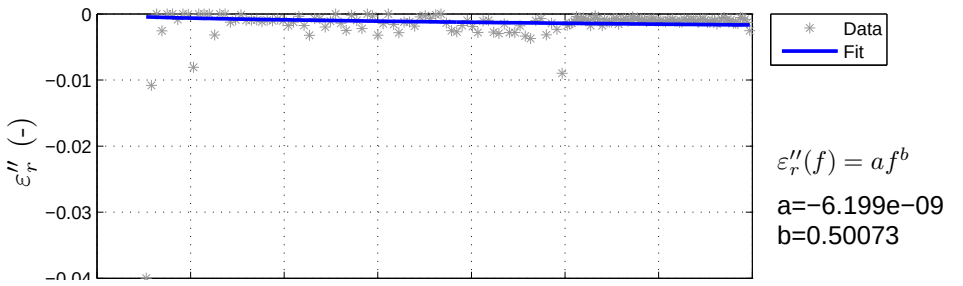
Data
Fit
ε_r'' (-)
$\varepsilon_r''(f) = af^b$
a=−6.199e−09
b=0.50073

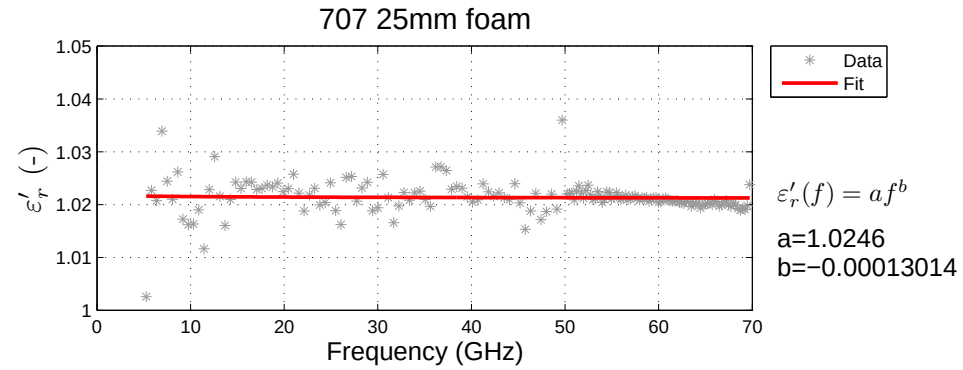
707 25mm foam
Data
Fit
ε_r' (-)
Frequency (GHz)
$\varepsilon_r'(f) = af^b$
a=1.0246
b=−0.00013014

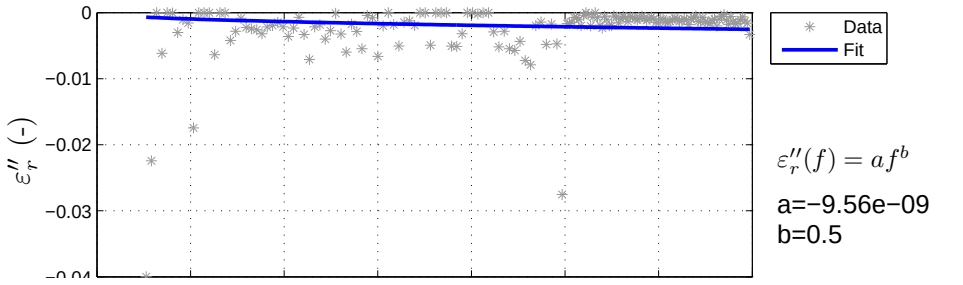
Data
Fit
ε_r'' (-)
$\varepsilon_r''(f) = af^b$
a=−9.56e−09
b=0.5

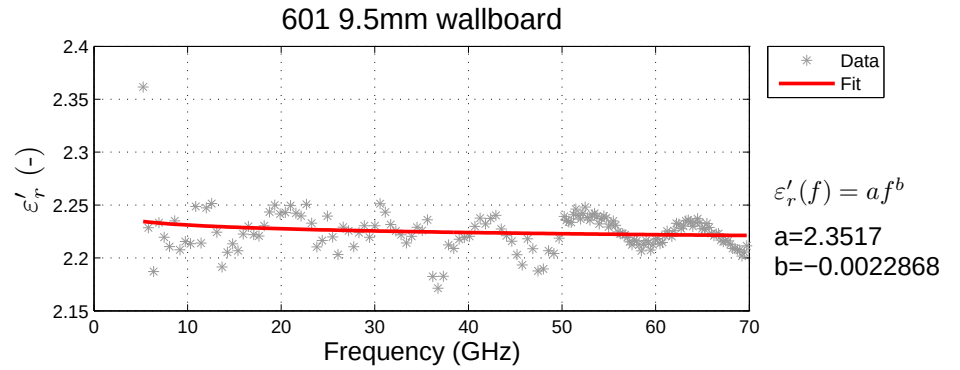
601 9.5mm wallboard
Data
Fit
ε_r' (-)
Frequency (GHz)
$\varepsilon_r'(f) = af^b$
a=2.3517
b=−0.0022868

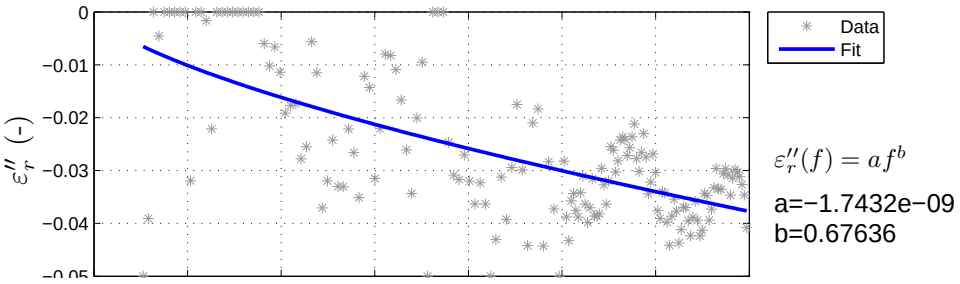
Data
Fit
ε_r'' (-)
$\varepsilon_r''(f) = af^b$
a=−1.7432e−09
b=0.67636

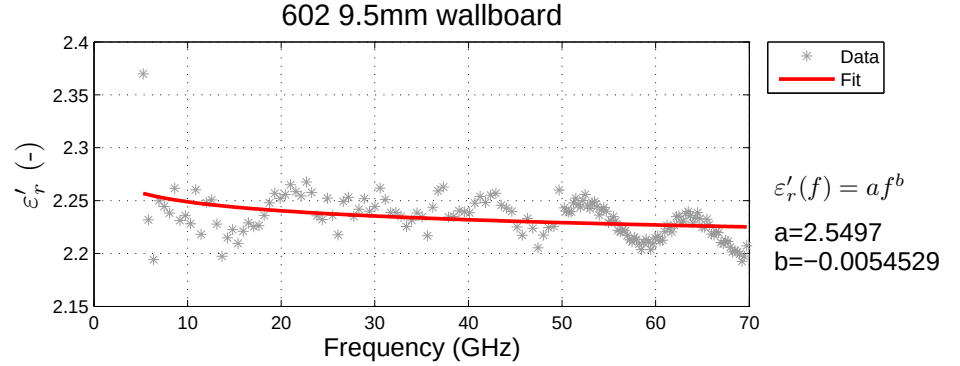
602 9.5mm wallboard
Data
Fit
ε_r' (-)
Frequency (GHz)
$\varepsilon_r'(f) = af^b$
a=2.5497
b=−0.0054529

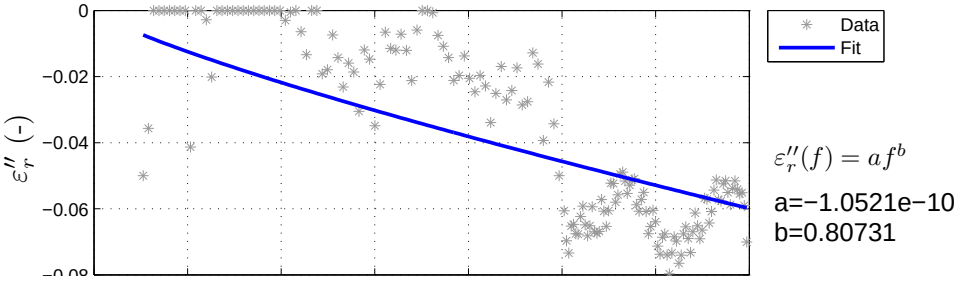
Data
Fit
ε_r'' (-)
$\varepsilon_r''(f) = af^b$
a=−1.0521e−10
b=0.80731

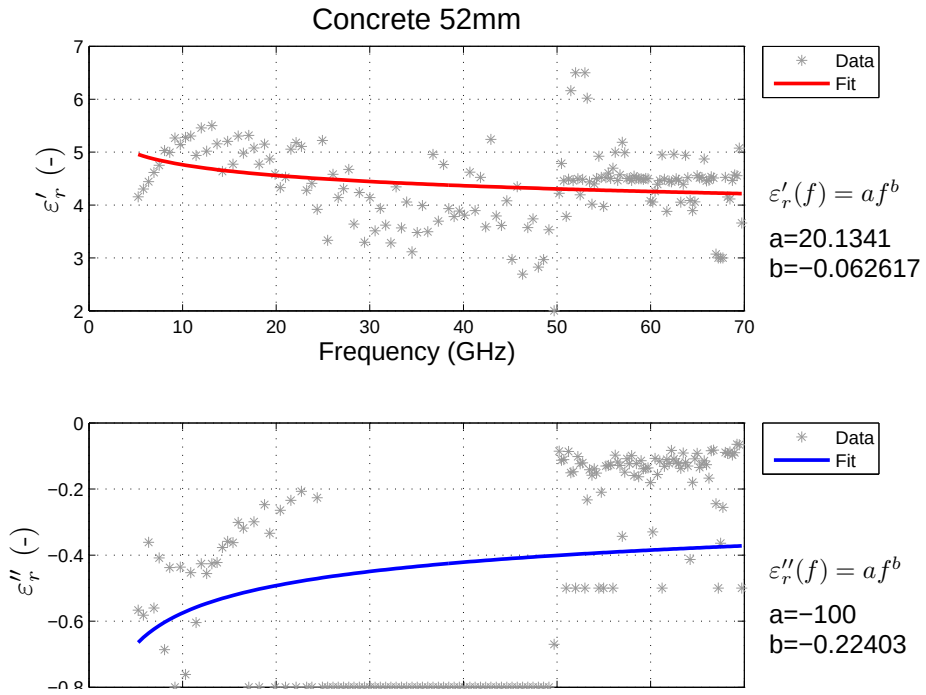
Concrete 52mm
Data
Fit
ε_r' (-)
Frequency (GHz)
$\varepsilon_r'(f) = af^b$
a=20.1341
b=−0.062617
Data
Fit
ε_r'' (-)
$\varepsilon_r''(f) = af^b$
a=−100
b=−0.22403

5 Discussion

5.1 The problem of two frequency bands

As mentioned in the Introduction, samples were measured in two frequency bands. Because of this, all samples had to be measured twice and the time between the measurements was several days. It could cause problems with reproducibility of the results caused by e.g. different temperature and humidity in the laboratory and different humidity of the samples. Finally, the antennas for the lower and upper band had different connectors and thus usage of different calibration kit was necessary. These mentioned facts led to discontinuous results in both bands.

Therefore $\varepsilon_r'(f)$, $\varepsilon_r''(f)$ were extracted in two frequency band separately and there is not a smooth transition between the traces for few samples at 50 GHz (see samples: B2, B3, G1, 102).

5.2 Limited dynamic range

Generally the free space measurement requires sufficient dynamic range but we had to rely on the output power produced by the VNA. Output power available on the VNA port in the upper band was approximately 3 dBm and in the lower band it was 10 dBm. If we take in account all the loss in our measurement setup (cables, adapters, free space loss) the dynamic range is insufficient for very lossy materials such as concrete for which we were unable to extract complex permittivity.

5.3 MUT reference plane offset

Difference between thickness of the reference metal sheet and thickness of the measured MUT had to be fixed by proper de-embedding which was performed to compensate the resulting offset length to achieve reliable extraction of the permittivity.

5.4 Fourier transform and time gating

The GRL calibration method relies on proper use of Fourier transformations. This is necessary to correctly switch between time-domain and frequency-domain data because the time gating is utilized to evaluate specific time-span from the reflected data. The Fourier transformations and gating have to be performed with suitable gate functions and window functions. The resulting calibrated data are very sensitive to the properties of the gate or window functions.

5.5 Antena – MUT distance

The used model derived in [9] assumes the impact of plane wave. This can be achieved by sufficiently separating the antennas and MUT or by using dielectric lenses. Because greater distance between antennas and MUT causes higher losses (longer cables, free space losses) we chose the compromise between sufficient dynamic range and planarity of wave in the antenna–MUT distance.

Figure 6: Detail of the layered material B3.

5.6 Inhomogeneous materials

By optical inspection (see Fig. 6) it was evident that materials B3 and B4 are composed from several different layers. Basically these materials are composed from two interleaved materials. Each layer is thinner than 2 mm which is comparable with $\lambda/2$ of frequencies above 60 GHz and therefore the physical model derived for homogeneous material should not be used in this case.

6 Summary

All material samples were successfully measured according to the original WP1 plan. The measurement data are available at CTU for publication and further processing if needed. The measurement system for the free space transmission and reflection measurements at 10-70 GHz is available at CTU for further experiments within the WiFEEB project.

References

[1] Faculty of Electronic and Electrical Engineering, University of Sheffield: "Materials Permittivity Table," original file: Materials Perm Table.docx, accessed 12th July 2012.

[2] "Miscellaneous dielectric constants," `http://www.microwaves101.com/encyclopedia/Miscdielectrics.cfm` accessed 22nd November 2012.

[3] Rohde&Schwarz GmbH&Co. KG, "R&S ZVA Vector Network Analyzer Specifications," `http://www2.rohde-schwarz.com/file_18299/ZVA_dat-sw_en.pdf` accessed 8th November 2012.

[4] Agilent Technologies Inc., "Basics of Measuring the Dielectric Properties of Materials," Application Note, 5989-2589EN, 2006.

[5] RFspin s.r.o., "Model DRH50 – Double Ridged Waveguide Horn," `http://www.rfspin.cz/en/antennas/drh50.php` accessed 8th November 2012.

[6] RPG Radiometer Physics GmbH, "WCA-75 – Coaxial to waveguide transitions."

[7] P. G. Bartley and S. B. Begley, "Improved Free-Space S-Parameter Calibration," *Instrumentation and Measurement Technology Conference*, 2005. IMTC 2005. Proceedings of the IEEE. vol. 1, pp. 372-375, 16-19 May 2005.

[8] A. Ferrero and U. Pisani, "Two-port network analyzer calibration using an unknown 'thru'," *IEEE Trans. Microw. Guid. Wave Lett.*, vol. 2, no. 12, pp. 505-507, Dec. 1992.

[9] B. Davis, C. Grosvenor, R. Johnk, D. Novotny, J. Baker-Jarvis, and M. Janezic, "Complex permittivity of planar building materials measured with and ultra-wideband free-field antenna measurement system," NIST J. Res., vol. 112, no. 1, pp. 67-73, Jan./Feb. 2007.

[10] J. Baker-Jarvis, E. J. Vanzura, W. A. Kissick, "Improved technique for determining complex permittivity with the transmission/reflection method," *IEEE Trans. Microw. Theory Tech.*, vol. 38, no. 8, pp. 1096-1103, Aug. 1990. doi: 10.1109/22.57336

[11] G. F. Engen and C. A. Hoer, "Thru-Reflect-Line: An Improved Technique for Calibrating the Dual Six-Port Automatic Network Analyzer," *IEEE Trans. Microw. Theory Tech.*, vol. MTT-27, no. 12, pp. 987-993, Dec 1979.